A Variable Temperature Neutron Diffraction Study of the Novel Oxide Ionic Conductor $Ba_3MoNbO_{8.5}$

Published title: Investigation of the relationship between the structure and conductivity of the novel oxide ionic conductor $Ba_3MoNbO_{8.5}$

S. Fop [1], E. J. Wildman, J. T. S. Irvine, P. A. Connor, J. M. S. Skakle [1], C. Ritter [1] and A. C. Mclaughlin[1]*

[1] Department of Chemistry, University of Aberdeen, Meston Walk, Aberdeen AB24 3UE, United Kingdom

[2] Institut Laue Langevin, 6 rue Jules Horowitz, BP 156, F-38042 Grenoble Cedex 9, France

*a.c.mclaughlin@abdn.ac.uk

Tel:0044 1224272924 Fax: 0044 1224272921

Abstract

A variable temperature neutron diffraction study of the novel oxide ion conductor $Ba_3MoNbO_{8.5}$ has been performed between 25 °C and 600 °C. Non-monotonic behaviour of the cell parameters, bond lengths and angles are observed indicating a structural rearrangement above 300 °C. The oxygen/vacancy distribution changes as the temperature increases so that the ratio of $(Mo/Nb)O_4$ tetrahedra to $(Mo/Nb)O_6$ octahedra increases upon heating above 300 °C. This unusual structural rearrangement results in relaxation of Mo(1)/Nb(1) and Ba(2) away from the mobile oxygen, enhancing the ionic conductivity. The second order Jahn-Teller effect most likely further enhances the distortion of the MO_4/MO_6 polyhedra as distortions created by both electronic and structural effects are mutually supportive.

Introduction

Oxide ion conductors have received much attention in recent years due to their application as solid oxide fuel cell (SOFC) electrolytes, solid oxide electrolyser cells (SOECs), oxygen sensors and oxygen separation membranes. SOFCs offer an efficient alternative to combustion technology for electricity production. The advantages of the high operating temperature for SOFCs include the possibility of running directly on practical hydrocarbon fuels without the need for complex and expensive external fuel reformer and purification systems. The high quality exhaust heat released during operation can be used as a valuable energy source, either to drive a gas turbine when pressurized or for combined heat and power (CHP) applications, so further increasing system efficiency.

So far several oxide ion conductors have been reported including fluorite-like systems [1], silicon and germanium apatites [2], $La_2Mo_2O_9$ (LAMOX) materials [3], $Bi_4V_2O_{11}$ derivatives (BIMEVOX) [4] and complex oxides with GaO_4 tetrahedral moieties [5]. To simplify certain materials issues, such as sealing and to enable the use of cheaper steel interconnects, it is desirable to lower the SOFCs' operating temperature from 800 ºC, to an intermediate range of 400 – 600 °C [6]. So far, materials that exhibit high conductivity at low temperature, such as aliovalent doped ceria or isovalent cation stabilised bismuth oxide, are less stable under the reducing fuel environment. The oxide ion conductivity of a material is strongly dependent on the crystal structure, hence in order to reach the objective of an intermediate temperature fuel cell it is important to discover new structural families of oxide ion conducting materials.

The perovskite structural family appears to offer great potential for the discovery of new oxide ion conductors due to its structural adaptability. Several perovskite materials with high oxide ion conductivity have been reported including strontium and magnesium-doped lanthanum gallates (LSGM) [7] and more recently the well-known ferroelectric material $Na_{0.5}Bi_{0.5}TiO_3$ [8] and

the perovskite derivative $NdBaInO_4$ [9]. We have recently identified a novel oxide ion conductor $Ba_3MoNbO_{8.5}$ [10] which exhibits a bulk conductivity of 2.2 x 10^{-3} S cm^{-1} at 600 °C. $Ba_3MoNbO_{8.5}$ crystallises in a hybrid of the 9R hexagonal perovskite and palmierite structures, which is a novel and so far unique crystal structure. Units of $(Mo/Nb)O_4$ and $(Mo/Nb)O_6$ coexist within the structure, forming a disordered arrangement of Mo/Nb tetrahedra and octahedra. $Ba_3MoNbO_{8.5}$ exhibits oxygen transport numbers of 0.99 in air/O_2 and 0.92 in air/5% H_2 in Ar at 600 °C, suggesting that $Ba_3MoNbO_{8.5}$ is an oxide ion conductor with negligible electrical conductivity in air/O_2 and that a small amount of electronic conduction is observed in air/5% H_2 in Ar. The phase is also surprisingly stable in 5 % H_2/N_2 [10]. $Ba_3MoNbO_{8.5}$ is the first hexagonal perovskite to display such promising transport numbers / oxide ion transport at low temperature. All other hexagonal systems previously reported exhibit mixed oxide ion and electronic and/or proton conductivity with low conductivities and low transport numbers [11]. In order to further investigate the conduction mechanism in $Ba_3MoNbO_{8.5}$ we have performed a variable temperature neutron diffraction study between 25 to 600 °C.

Experimental

Stoichiometric amounts of $BaCO_3$ (99.999%, Aldrich), MoO_3 (99.5+%, Aldrich) and Nb_2O_5 (99.99%, Aldrich) were ground, pressed into 13 mm pellets and calcined in an alumina crucible at 900 °C for 10 hours. The pellets were subsequently reground, pelleted and heated at 1100 °C for 48 hours and then cooled to room temperature at 5 °C/min. The latter heating step was repeated until phase pure products were obtained.

Variable temperature neutron diffraction patterns in the temperature range 25 to 600 °C were recorded on the high-resolution powder diffractometer D2B at the Institut Laue-Langevin (ILL) in Grenoble, France. A sample of 5 grams of $Ba_3MoNbO_{8.5}$ was inserted in an open quartz tube and heated up to the desired temperatures. Data were collected at λ = 1.59432 Å with a total collection time of 2.5 hours for each temperature step.

For the impedance spectroscopy measurements, a pellet of ~ 10 mm diameter and ~ 1.5 mm thickness was prepared from a powder sample of $Ba_3MoNbO_{8.5}$ and sintered at 1100 °C for 48 hours (to achieve > 95 % of the theoretical density). Pt electrodes were painted on both sides of the pellet using a Pt-paste (Metalor 6082). Impedance spectra were recorded with a Solartron 1260 impedance analyser in the frequency range 0.1 Hz – 1 MHz with an applied alternating voltage of 0.1 V. Data were recorded upon cooling from 600 °C to 300 °C in a sealed tube furnace under the flow of dry air, measuring every 15 °C and allowing 2 hours of equilibration at each temperature step. The obtained data were corrected by the geometrical factor of the sample and treated with the ZView software (Scribner Associates, Inc.).

Results and Discussion

Neutron diffraction data at all temperatures were fitted by the Rietveld method using the GSAS/EXPGUI program [12, 13]. Modelling of the background was performed by the shifted Chebyschev polynomial function and the peak shapes were fitted using a Pseudo-Voigt function. The hybrid 9R polytype – palmierite model previously reported [10] (Figure 1) was used as a starting model for the variable temperature refinements. This model is formed by a disordered arrangement of Mo and Nb cations in mixed tetrahedral – octahedral coordination, which is created by the occupation of both the 9*e* (9R polytype) and 6*c* (palmierite) oxygen positions. Oxygen atoms are present at three different Wyckoff sites: O(1) in 18*h*, O(2) in 9*e* and O(3) in 36*i*; the latter position is employed instead of 6*c* to take into account the dynamic disorder evidenced by the large U_{11}, U_{22} and U_{12} values for O(3) found in the previous structural refinement [10]. Mo/Nb cations (M) are in 6*c* and 3*b*, while the Ba atoms occupy the 6*c* and 3*a* sites.

An excellent fit to the neutron data was obtained with the hybrid model described above for all temperatures (the refined data recorded at 25 °C and 600 °C are displayed in Figure 2). There is no evidence of peak splitting or superstructure peaks and the $R\bar{3}m$ H symmetry is observed

over the whole temperature range. The refined atomic positions and agreement indices are displayed in Table 1. The atomic displacement parameters, U_{ij}, were refined anisotropically for all atoms except O(3), for which an U_{iso} parameter was used as previously reported [10]. Attempts to independently refine the M(1) and M(2) U_{ij} parameters generated unrealistic U_{33} values; therefore the U_{ij} parameters of the M atoms on the 6*c* and 3*b* sites were constrained to be the same. The displacement parameters for all atoms are reported in Table 1. The atomic U_{ij} anisotropic values generally increase with the temperature as expected. Overall, the obtained thermal displacement values are within the range expected for this type of material, with similar values being found for α- and β-$La_2Mo_2O_9$ [14], γ-$Bi_4V_2O_{11}$ [15], $La_{1.54}Sr_{0.46}Ga_3O_{7.27}$ [16], and LSGM materials [17]. The large U_{33} values indicate that the M cations exhibit motion mainly parallel to the *c*-axis. Ba(1) presents $U_{11} = U_{22} > U_{33}$, indicating preferential thermal motion on the *ab* plane. On the contrary, the Ba(2) atom shows larger U_{33} values, evidencing anisotropic motion along the *c*-axis. Ba(1) is encircled by a belt of O(2) and O(3) sites, while Ba(2) and M(1) are directly above (or below) the O(2) and O(3) positions. The distribution of occupied/unoccupied O(2) and O(3) sites creates different coordination environments for the metal cations, thus inducing motion on the *ab* plane (Ba(1)) or along the *c*-axis (Ba(2) and M(1)). The O(1) thermal ellipsoids are oriented perpendicularly to the M–O bonds. The O(2) ellipsoids are nearly spherical in the whole temperature range and O(3) exhibits large U_{iso} values as previously reported [10].

The temperature dependency of the *a* and *c* cell parameters are shown in Figure 3 and non-monotonic behaviour is observed. A clear change in slope of both *a* and *c* is observed above 300 °C suggesting a possible structural modification. The fractional occupancies of the atoms in the structural model obtained previously [10] were used as starting values for the refinement of the variable temperature neutron diffraction data. The Ba and O(1) fractional occupancies refined to within ± 1% of full occupancy and were fixed at 1.0. The occupancies of the other

atoms were refined from their initial values. The refined fractional occupancies are presented in Table 1. Figure 4 shows the temperature dependency of the fractional occupancies of M(1), M(2), O(2) and O(3). There is little change in the fractional occupancies between 25 °C - 300 °C. Above this temperature a sudden increase in the M(1) fractional occupancy, with a concomitant decrease in the M(2) fractional occupancy, is evidenced. The same behaviour is observed for the O(2) and O(3) fractional occupancies, which respectively decrease and increase above 300 °C. Above 500 °C there is little variation in the fractional occupancies of M(1), M(2), O(2) and O(3). An overall oxygen stoichiometry of 8.5 was obtained at all temperatures.

Ba(1), Ba(2) and O(1) form the rigid part of the $Ba_3MoNbO_{8.5}$ structure, while M(1), M(2), O(2) and O(3) are responsible for the variable tetrahedral/octahedral coordination. Therefore, changes in the occupancies of the latter atoms indicate that the structure is able to adjust the ratio of tetraheda to octahedra and, consequently, oxygen/vacancy distributions as the temperature increases. The results demonstrate that the number of $(Mo/Nb)O_4$ tetrahedra increases upon heating above 300 °C. The mutual self-rearrangement of the Mo/Nb and oxygen occupancies is striking evidence of the ability of the metal lattice to support variable coordinations. It has been demonstrated that the presence of flexible *d*-metal cations is essential for the ionic transport of various oxide ion conductors. The high oxygen conduction of β-$La_2Mo_2O_9$ is thought to be facilitated by the capacity of the molybdenum atom to assume co-ordinations between 4 and 6 [13, 18]. In the BIMEVOX materials the oxygen motion proceeds through the decomposition and reformation of the V–O units on the perovskite layers. An oxygen atom is transferred from a VO_6 octahedron to a vacancy contained in a nearby $V'O_4$ tetrahedron, forming a short-living $VO_5V'O_5$ complex. The complex then separates into a VO_4 tetrahedron and a $V'O_6$ octahedron, completing the oxygen migration [19]. In the same way, $Ba_3MoNbO_{8.5}$ possesses a flexible lattice in which the M atoms are readily able to change

coordination, creating a potential avenue for conduction as it is possible for an oxide ion to migrate from one $M(1)O_X$ unit to the other.

Selected bond lengths and angles for $Ba_3MoNbO_{8.5}$ at the various temperatures are displayed in Table 2. Information on how the M polyhedra respond to the oxygen/vacancy rearrangement can be obtained by following some key bond lengths and angles. Figure 5 (b) shows a superimposition of the coordination of the $M(1)–O(1)_3O(3)$ tetrahedra and the $M(1)–O(1)_3O(2)_3$ octahedra. $M(1)–O(1)_3O(3)$ and $M(1)–O(1)_3O(2)_3$ share the same $M(1)O(1)_3$ unit, which presents three equal M(1)–O(1) bond lengths and three equal O(1)–M(1)–O(1) angles (α). $M(1)–O(1)_3O(3)$ is then defined by the M(1)–O(3) bond length and the O(1)–M(1)–O(3) angle (β), obtained by the average of the three possible angles given by the O(3) split position. The $M(1)–O(1)_3O(2)_3$ octahedron is defined by the M(1)–O(1) bond length, α, the M(1)–O(2) bond lengths and the O(1)–M(1)–O(2) and O(2)–M(1)–O(2) angles (γ and δ respectively). The temperature dependencies of the distances and angles defined above are displayed in Figure 5. All of the bond lengths and angles exhibit little variation with temperature below 300 °C but evidence a sizeable change between 300 °C – 500 °C. Between 300 °C – 500 °C there is an increase in α and decrease in γ, β and δ. The M(1)–O(1) bond length contracts whilst both M(1)–O(3) and M(1)–O(2) expand (Table 2, Figure 5). The thermal modifications of the M(1) polyhedron are reflected to the neighbouring $M(2)O(1)_6$ octahedron where the M(2)–O(2) bond lengths and the O(1)–M(2)–O(1) angles both increase with the temperature resulting in a net expansion of the $M(2)O(1)_6$ octahedra.

$Ba_3MoNbO_{8.5}$ presents a peculiar thermal variation of the cell parameters, bond lengths and angles. These quantities exhibit nonlinear behaviour, with abrupt changes between 300 °C and 500 °C. The $Ba_3MoNbO_{8.5}$ structure relaxes in response to the rearrangement of the oxygen/vacancy distribution. The M(1) polyhedra are already distorted at 25 °C [10] (Table 2), due to the effect of the second order Jahn-Teller distortion [20]. Examination of the variation of

the M(1)–O distances and angles with temperature indicates further displacement of the M(1) atom away from the O(2)/O(3) sites, towards the [O(1)-O(1)-O(1)] face of the M(1)–$O(1)_3$ unit (Figure 5). The magnitude of the displacement (*D*) can be obtained by calculation of the distance between M(1) and the [O(1)-O(1)-O(1)] face. This is given by D = -M(1)–O(1)cos(β) and the displacement can be evaluated by the difference between the M(1)–[O(1)-O(1)-O(1)] distance at temperature, T, and the M(1)–[O(1)-O(1)-O(1)] distance at 25 °C. The M(1) displacement is plotted against the temperature in Figure 5(c). The results clearly demonstrate that the variation of the oxygen/vacancy distribution between 300 – 500 °C strongly affects the relaxation of the M–O framework. We note that the second order Jahn-Teller effect previously reported for $Ba_3MoNbO_{8.5}$ [10] may further enhance the distortion of the MO_4/MO_6 polyhedra, as distortions created by both electronic and structural effects are mutually supportive [19]. The Ba lattice relaxes in a similar way, with Ba(2) displacing away from O(2)/O(3).

Displacement of the metal atoms of the cationic lattice away from the mobile oxide ions has been reported in several different oxide ion conductors. In doped $LaGaO_3$ perovskites, La and B-site cations shift away from the mobile oxygen atom [21]. Similarly, the Si atoms in the $La_{9.33}Si_6O_{26}$ apatite move away from the channels in which migration of the interstitial oxygen atoms occurs [22]. In $Ba_3MoNbO_{8.5}$, the average M(1) displacement is an effect of the rearrangement of the oxygen/vacancy distribution at the O(2) and O(3) sites but can also be correlated to the energetics of the ionic conduction as displacement of *d*-metal cations from oxygen vacancies in the lattice is thought to lower the motional enthalpy required for the mobility of the oxide ions [23]. The average structural relaxation, obtained from the neutron diffraction data, is therefore most likely a consequence of both the structural rearrangement and the dynamic and local structural reorganisation induced by the oxygen hopping.

The oxide ionic conductivity is thought to arise in the $Ba(1)O(2,3)_{2.5}$ layer. The O(2) and O(3) sites are partially occupied and the short distance between the 9*e* and 36*i* positions (< 2.2 Å)

excludes simultaneous occupancy of adjacent O(2) and O(3) sites. This leads to a random distribution of vacancies on the $Ba(1)O(2,3)_{2.5}$ layer, which are available for the ionic migration. The partially occupied O(2) and O(3) sites on the $Ba(1)O(2,3)_{2.5}$ layers are distributed in a zigzag fashion inside channels created by the rigid Ba(1), Ba(2) and O(1) framework. This channels propagate in the [100], [010] and [110] directions and might provide possible conduction pathways. It is most likely that the movement of oxide ions is via octahedral and tetrahedral interchange and suggests a cooperative motion such as an interstitialcy mechanism.[10]. This process is assisted by the ability of the system to locally and dynamically reorganise its oxygen/vacancy distribution. Between 300 °C and 500 °C it is proposed that the increase in the number of tetrahedra, coupled with the displacement of M(1) and Ba(2) away from O(2) and O(3) enhances the electrical properties, so that a conductivity comparable to other leading solid oxide ion conductors is observed. The presence of both the structural modification above 300 °C and the second order Jahn-Teller distortion are important for oxide ion conduction in $Ba_3MoNbO_{8.5}$. Both effects result in displacement of the the Mo/Nb away from the migrating O^{2-} ions and will reduce the migration energy. It may be possible to tune the ionic conduction further by enhancing the Jahn-Teller distortion further by replacing Nb^{5+} with V^{5+}. Furthermore the increase in the number of $(Mo/Nb)O_4$ tetrahedra above 300 °C most likely offers more low energy transition paths for transport of the O^{2-} ions, further enhancing the conductivity. The preference for a tetrahedral environment gives a large number of possible oxygen positions which are important for collective mechanisms involving strongly correlated motions of sets of tetrahedral as previously observed for brownmillerite $Ba_2In_2O_5$ [24] The Arrhenius plot of the bulk conductivity of $Ba_3MoNbO_{8.5}$ is presented in the inset to Figure 5 (c). The bulk conductivity is 2.2 x 10^{-3} S cm^{-1} at 600 °C with an activation energy of 1.211 (6) eV for temperatures between 300 – 500 °C. There is a clear correlation between the change in the crystal lattice and the electrical properties at temperatures > 500 °C (Figure 5). Between

300 °C and 500 °C the rearrangement of M(1), M(2), O(2) and O(3) within the crystal structure results in an increase of the ratio of MO_4 tetrahedra to MO_6 octahedra with concomitant changes in the bond lengths and angles. Above 500 °C there is little change in the structural parameters. At the same temperature a change in slope is evidenced in the Arrhenius plot with the activation energy lowering to 0.71 (1) eV

The motional enthalpy, ΔH_m, directly contributes to the activation energy of the conduction process and is the sum of two components: a barrier energy for the ionic hopping and a relaxation energy needed for the lattice relaxation around the conductive sites [25]. Displacement of *d*-metal cations from oxygen vacancies in the lattice is thought to lower the motional enthalpy required for the mobility of the oxide ions [22]. Therefore, the change in activation energy of the bulk conductivity of $Ba_3MoNbO_{8.5}$ above 500 °C (Figure 5(c)) can be correlated to the M(1) displacement. For T ≥ 500 °C, M(1) has reached its maximum displacement and the ionic transfer happens with a lower motional enthalpy, thus reducing the activation energy to 0.71 (1) eV.

Conclusions

In summary this variable temperature neutron diffraction study demonstrates an unusual structural rearrangement in $Ba_3MoNbO_{8.5}$ between 300 °C and 500 °C so that the ratio of tetraheda to octahedra increases and, consequently the oxygen/vacancy distribution changes as the temperature increases. We propose that the conductivity is enhanced by the increase in the proportion of MO_4 tetrahedra between 300 °C and 500 °C and that substitution of Nb^{5+} with an aliovalent cation with preferential tetrahedral co-ordination may be a way to further optimise the conductivity at low temperature in $Ba_3MoNbO_{8.5}$. The change in vacancy distribution combined with the oxide ion migration results in displacement of M(1) and Ba(2) lattice away from the mobile oxygen, lowering the motional enthalpy required for the mobility of the oxide ions and enhancing the conductivity. Above 500 °C the structural rearrangement and

subsequent relaxation of the cationic lattice appears complete so that the activation energy reduces to 0.71 (1) eV.

References

[1] Kuang, X., Payne, J. L., Johnson, M. R. & Radosavljevic, I. E. *Angew. Chemie - Int. Ed.* **51**, 690–694 (2012).

[2] Kendrick, E., Islam, M. S. & Slater, P. R. *J. Mater. Chem.* **10**, 3104–3111 (2007).

[3] Lacorre, P., Goutenoire, F., Bohnke, O., Retoux, R. & Laligant, Y. *Nature* **404**, 856–858 (2000).

[4] Abraham, F., Debreuille-Gresse, M. F., Mairesse, G. & Nowogrocki, G. *Solid State Ionics* **30**, 529–532 (1988).

[5] Kuang, X. *et al. Nat. Mater.* **7**, 498–504 (2008).

[6] Wachsman, E. D. & Lee, K. T. *Science* **334**, 935–9 (2011).

[7] T. Ishihara, H. Matsuda & Y. Takita. *J. Am. Chem. Soc.* **116**, 3801–3803 (1994).

[8] Li, M. *et al. Nat. Mater.* **13**, 31–5 (2014).

[9] Fujii, K. *et al. Chem. Mater.* **26**, 2488–2491 (2014).

[10] Fop, S. Skakle, J. M. S., Mclaughlin, A. C., Connor , P., Irvine, J. T. S., Smith, R. I. & Wildman, E. J. *J. Am. Chem. Soc.* **138**, 51 (2016).

[11] Kuang, X, Allix, M., Ibberson, R. M., Claridge, J. B., Niu, H. & Rosseinsky, M. J. *Chem. Mater.* **19**, 2884–2893 (2007); Ling, C. D. *et al*, *Chem. Mater.* **21**, 3853–3864 (2009).

[12] A. C. Larson and R. B. Von Dreele, "General structure analysis system (GSAS)", Los Alamos National Laboratory Report LAUR 86-748 (1994).

[13] B. H. Toby, "EXPGUI, a graphical user interface for GSAS", *J. Appl. Cryst.*, **34** (2001), 210.

[14] I. R. Evans, J. A. K. Howard amd J. S. O. Evans, "The crystal structure of α- $La_2Mo_2O_9$ and the structural origin of the oxide ion migration pathway", *Chem. Mater.*, **17** (2005), 4074.

[15] G. Mairesse, P. Roussel, R. N. Vannier, M. Anne, C. Pirovano and G. Nowogrocki, "Crystal structure determination of α, β, and γ-$Bi_4V_2O_{11}$ polymorphs. Part I: γ and β-$Bi_4V_2O_{11}$", *Solid State Sci.*, **5** (2003), 851.

[16] X. Kuang, M. A. Green, H. Niu, P. Zajdel, C. Dickinson, J. B. Claridge, L. Jantsky and M. J. Rosseinsky, "Interstitial oxide ion conductivity in the layered tetrahedral network melilite structure", *Nature Mater.*, **7** (2008), 498.

[17] M. Kajitani, M. Matsuda, A. Hoshikawa, S. Harjo, T. Kamiyama, T. Ishigaki, F. Izumi and M. Miyake, "In situ neutron diffraction study of fast oxide ion conductor $LaGaO_3$-based perovskite compounds", *Chem. Mater.*, **17** (2005), 4235.

[18] F. Goutenoire, O. Isnard, R. Retoux and P. Lacorre; "Crystal structure of $La_2Mo_2O_9$, a new fast oxide-ion conductor", *Chem. Mater.*, **12** (2000), 2575.

[19] I. Abrahams and F. Krok, "Defect chemistry in the BIMEVOXes", *J. Mater. Chem.*, **12** (2002), 3351.

[20] M. Kunz and D. I. Brown, Out-of-center distortions around octahedrally coordinated d^0 transition metals, *J. Solid State Chem.* **115** (1995), 395.

[21] M. S. Islam, "Ionic transport in ABO_3 perovskite oxides: a computer modelling tour", *J. Mater. Chem.*, **10** (2000), 1027.

[22] M. S. Islam, J. R. Tolchard and P. R. Slater, "An apatite for fast oxide ion conduction", *Chem. Commun.*, **13**, (2003), 1486.

[23] J. B. Goodenough, A. Manthiram, M. Paranthamam and Y. S. Zhen, "Oxide ion electrolytes", *Mat. Sci. Eng. B-Solid*, **B12** (1992), 357.

[24] S. Stølen, E. Bakken and C. E. Mohn, *Phys. Chem. Chem. Phys.* **8** (2006), 429.

[25] J. B. Goodenough, "Oxide-ion electrolytes", *Annu. Rev. Mater. Res*., **33** (2003), 91.

Figure Captions

Figure 1. Crystal structure of $Ba_3MoNbO_{8.5}$. The hybrid structural model formed by the superimposition of the 9R-polytype and the palmierite sub-units representing the average structure of the system. Colours indicate: light green Ba(1), dark green Ba(2), blue Mo(1)/Nb(1), cyan Mo(2)/Nb(2), red O(1), orange O(2) and yellow O(3).

Figure 2. Rietveld refinement fit to the variable temperature neutron diffraction data of $Ba_3MoNbO_{8.5}$. Rietveld refinement fits of neutron diffraction data collected at 25 °C and 600 °C are shown. Black dots indicate the observed data, the red line the Rietveld fit, the blue line the difference between the observed and the calculated patterns, the green line the background function and the pink bars are the reflection positions.

Figure 3. Unit cell dimensions of $Ba_3MoNbO_{8.5}$. Thermal dependency of the *a*- and *c*-axis of the unit cell of $Ba_3MoNbO_{8.5}$. The linear fits evidence the change in slope between 300 °C and 400 °C.

Figure 4. Variation of fractional occupancies with the temperature. Temperature dependency of the fractional occupancies of M(1) and M(2) and O(2) and O(3). Connecting lines are guides for the eye only.

Figure 5. Thermal relaxation of the M(1) polyhedra. (a) Temperature dependency of selected bond distances and angles for the M(1) polyhedra. **(b)** Representation of the M–O lattice relaxation; black arrows show the modifications of the bond lengths and angles at 600 °C from the "equilibrium" values at 25 °C. The red arrow represents the average M(1) displacement. **(c)** Variation of the M(1) displacement with the temperature; the inset shows a scheme of the calculation of the distance (*d*) between M(1) and the [O(1)-O(1)-O(1)] plane of the M(1) polyhedron. In **(a)** and **(c)** lines are guides for the eyes only. Colours in **(b)** and **(c)** indicate: blue M(1), cyan M(2), red O(1), orange O(2) and yellow O(3).

Fig. 1

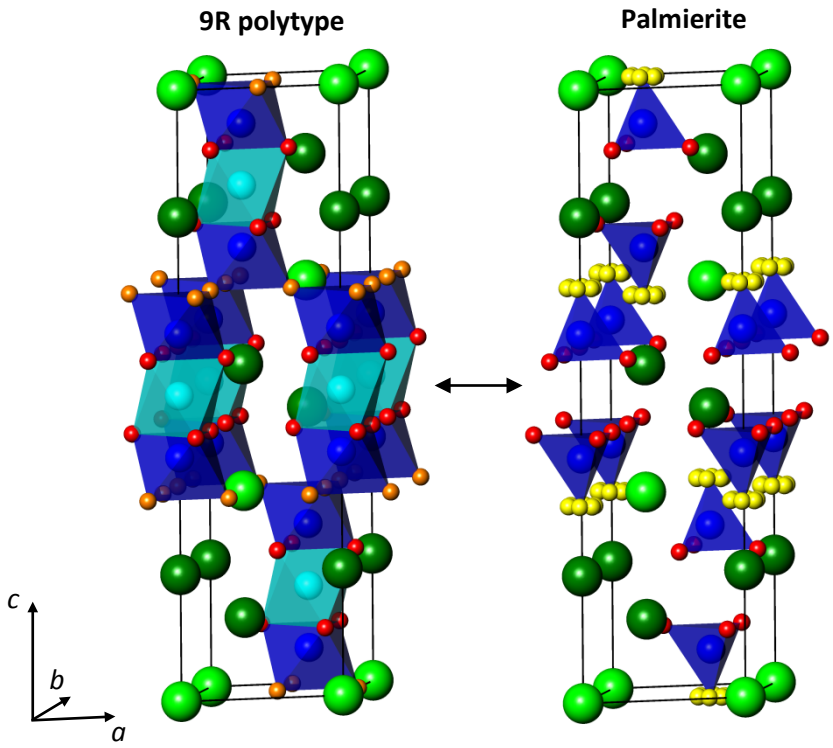

Figure 2

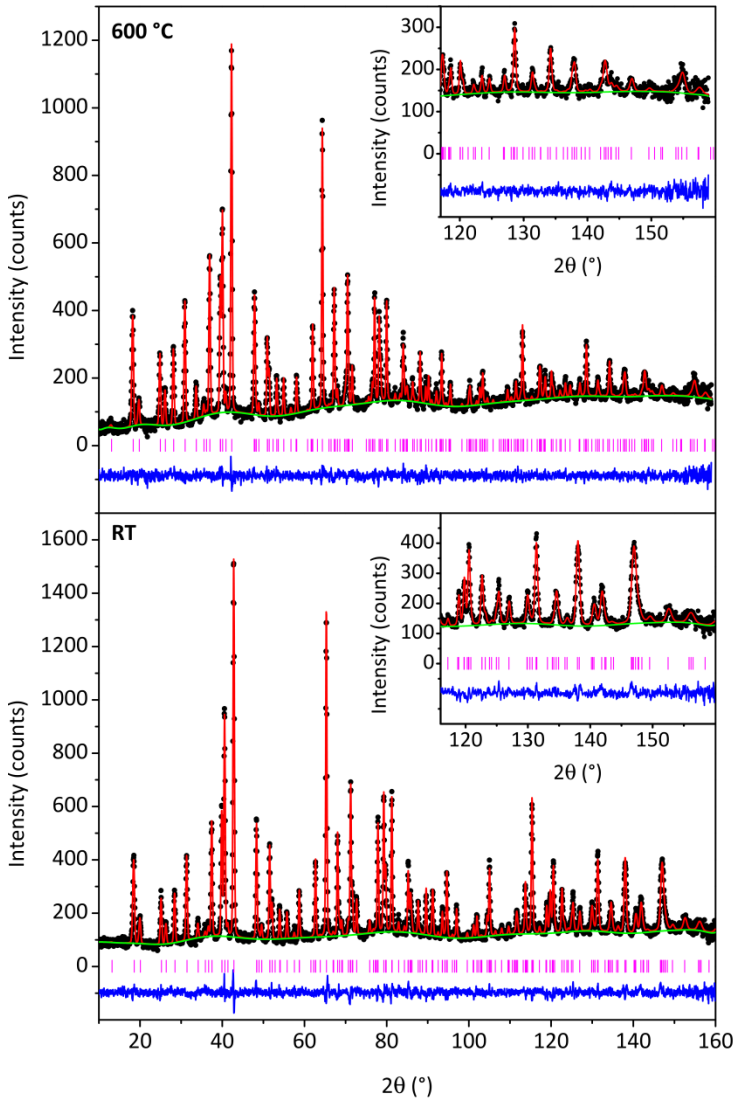

Figure 3

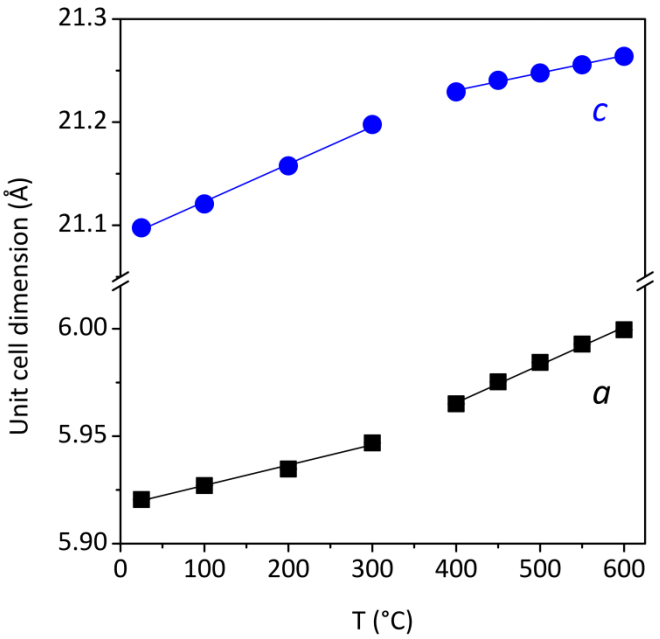
21.3
21.2
21.1
6.00
5.95
5.90
Unit cell dimension (Å)
c
a
0
100
200
300
400
500
600
T (°C)

Figure 4

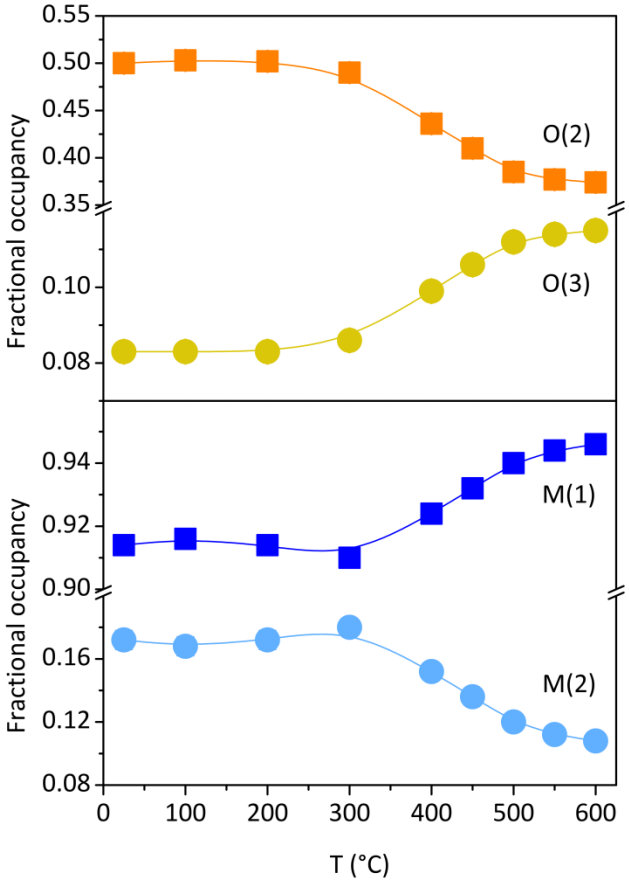
0.55
0.50
0.45
0.40
0.35
0.10
0.08
Fractional occupancy
O(2)
O(3)
0.94
0.92
0.90
0.16
0.12
0.08
Fractional occupancy
M(1)
M(2)
0
100
200
300
400
500
600
T (°C)

Figure 5

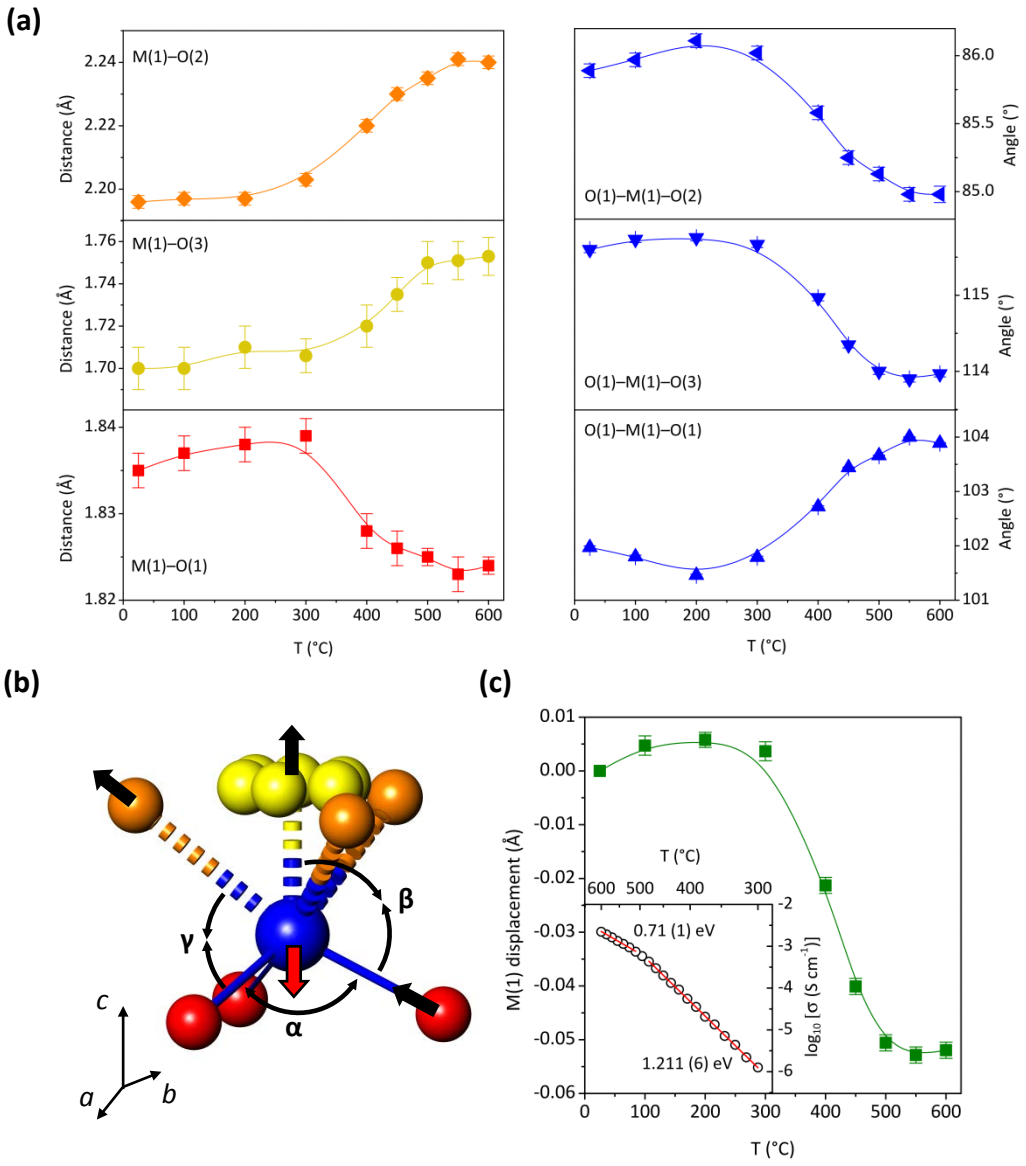
(a)
M(1)–O(2)
M(1)–O(3)
M(1)–O(1)
Distance (Å)
O(1)–M(1)–O(2)
O(1)–M(1)–O(3)
O(1)–M(1)–O(1)
Angle (°)
T (°C)
(b)
β
γ
α
c
a
b
(c)
M(1) displacement (Å)
T (°C)
0.71 (1) eV
1.211 (6) eV
log10 [σ (S cm-1)]